Exploration of the Potential Energy Surface of $C_9H_9^+$ by ab Initio Methods. 1. The Barbaralyl Cation

Dieter Cremer,*,† Peder Svensson,‡ Elfi Kraka,† and Per Ahlberg*,‡

Contribution from the Departments of Theoretical Chemistry and Organic Chemistry, University of Göteborg, Kemigården 3, S-41296 Göteborg, Sweden

Received October 16, 1992

Abstract: The potential energy surface (PES) of $C_9H_9^+$ has been explored in the region of the 9-barbaralyl cation (**3**) at MP2/-, MP3/-, and MP4(SDQ)/6-31G(d). Calculations show that **3** is 6.9 and 4.6 kcal/mol more stable than the nonclassical barbaralyl cation with D_{3h} symmetry (**5**) and the bicyclo[3.2.2]nona-3,6,8-trien-2-yl cation (**4**), respectively. The PES in the vicinity of **3** is rather flat and characterized by a spider network of reaction paths that connect 181 440 different forms of **3** with 90 720 different forms of **4** and 30 240 forms of **5**. Both **4** and **5** will not be accessible to experiment, since they sit either at a transition state (TS) or in a very shallow minimum surrounded by TSs of similar energy. This is in line with the McIver–Stanton symmetry rules for TSs. The energetically most favorable reactions of **3** are sixfold degenerate rearrangements via C_2 symmetrical TSs **8**, representing an activation energy of just 3.6 kcal/mol. Completely degenerate rearrangements of **3**, that lead to an equilibration of all C atoms of **3**, proceed via a novel type of mechanism that is characterized by *double-bifurcation reactions with three directly connected first-order TSs*, namely TS **8**, TS **4** as the barrier-determining TS, and another TS **8**. According to calculated geometrical parameters, IGLO/6-31G(d) ^{13}C chemical shifts, and MP2/6-31G(d) response densities, the chemical behavior of **3** is dominated by the stereocomposition of a cyclopropylcarbinyl cation unit in conjugation with two vinyl groups. Four of the nine formal single bonds of **3** are partial bonds with bond orders of just 0.8 and 0.5.

1. Introduction

In a continuous effort to investigate potentially homoaromatic ions and their properties by ab initio methods,[1,2] we present here the first study of the potential energy surface (PES) of the $C_9H_9^+$ ion utilizing correlation-corrected ab initio methods. In particular, we describe those areas of the PES which host the potentially homoaromatic 1,4-bishomotropylium cation (**1**)[3,4] and its classical counterpart, the *cis*-8,9-dihydro-1-indenyl cation (**2**) (see Scheme I). Another target of our study is the 9-barbaralyl cation (**3**) that is known to undergo both degenerate and nondegenerate rearrangements which may involve, either as intermediates or as transition states (TS), the bicyclo[3.2.2]nona-3,6,8-trien-2-yl cation (**4**) and the nonclassical barbaralyl cation structure **5**, in which positions 3, 7, and 9 (1, 2, 4, 5, 6, and 8) are equivalent by symmetry and which, accordingly, possesses D_{3h} symmetry (see Scheme I).[5–20] Structures **6–12** of Scheme I could present alternative TSs in degenerate rearrangements of **3**, and accordingly, they will also be discussed in this work.

A key experiment in the study of barbaralyl cations is the reaction of bicyclo[3.2.2]nona-3,6,8-trien-2-ol with superacid (Scheme II).[5–10] At −135 °C a sharp singlet can be observed in the ^1H NMR spectrum (δ = 6.6 ppm) that suggests either a regular planar nonagon with nine equivalent CH groups (which could only be an open shell system with 8π electrons and which can easily be excluded) or a rapidly rearranging cation that exchanges all its nine CH groups. The possibility that the nine CH groups occupy the corners of a convex regular polyhedron (a Platonian body) is excluded, since there exists no such polyhedron with nine corners. On the basis of ^{13}C NMR measurements, isotopic perturbation studies, and quantum chemical calculations, Ahlberg and co-workers[5–8,16] have provided reasons to exclude **4** and **5** and to assign structure **3** to the cation intermediate. In addition, these authors have suggested that **3** undergoes two different degenerate rearrangements A and B (shown in Figure 1) that lead to a complete scrambling of all nine C atoms. According to dynamic NMR measurements, the completely degenerate rearrangement of **3**, which leads to a ^1H signal at 6.6 ppm and a ^{13}C signal at 118.5 ppm at −135 °C, should possess a barrier of 5.0 kcal/mol.[5–8]

When the temperature is decreased to −150 °C, **3** continues to rearrange but rearrangements proceed via process A as the

† Department of Theoretical Chemistry.
‡ Department of Organic Chemistry.

(1) Cremer, D.; Reichel, F.; Kraka, E. *J. Am. Chem. Soc.* **1991**, *113*, 9459.
(2) Svensson, P.; Reichel, F.; Ahlberg, P.; Cremer, D. *J. Chem. Soc., Perkin Trans. 2* **1991**, 1463.
(3) See Part 2: following paper in this issue.
(4) (a) Ahlberg, P.; Harris, D. L.; Winstein, S. *J. Am. Chem. Soc.* **1970**, *92*, 2146. (b) Ahlberg, P.; Harris, D. L.; Roberts, M.; Warner, P.; Seidl, P.; Sakai, M.; Cook, D.; Diaz, A.; Dirlam, J. P.; Hamberger, H.; Winstein, S. *J. Am. Chem. Soc.* **1972**, *94*, 7063. (c) Engdahl, C.; Ahlberg, P. *J. Chem. Res., Synop.* **1977**, 342.
(5) Ahlberg, P.; Harris, D. L.; Winstein, S. *J. Am. Chem. Soc.* **1970**, *92*, 4454.
(6) (a) Engdahl, C.; Jönsäll, G.; Ahlberg, P. *J. Chem. Soc., Chem. Commun.* **1979**, 626. (b) Ahlberg, P.; Engdahl, C.; Jonsäll, G. *J. Am. Chem. Soc.* **1981**, *103*, 1583.
(7) Engdahl, C.; Jonsäll, G.; Ahlberg, P. *J. Am. Chem. Soc.* **1983**, *105*, 891. As discussed in this reference, the value of 3.8 kcal/mol is an upper limit to the true value.
(8) For a review on degenerate rearrangements of $C_9H_9^+$ ions, see: Ahlberg, P.; Jonsäll, G.; Engdahl, C. *Adv. Phys. Org. Chem.* **1983**, *19*, 223.
(9) Jonsäll, G.; Ahlberg, P. *J. Chem. Soc., Chem. Commun.* **1984**, 1125.
(10) For related reviews, see: (a) Olah, G. A.; Reddy, V. P.; Prakash, G. K. S. *Chem. Rev.* **1992**, *92*, 69. (b) Saunders, M.; Jimenez-Vazquez, H. A. *Chem. Rev.* **1991**, *91*, 375. (c) Leone, R. E.; Barborak, J. C.; Schleyer, P. v. R. In *Carbonium Ions*; Olah, G. A., Schleyer, P. v. R., Eds.; Wiley-Interscience: New York, 1973; Vol. 4, p 1837.
(11) (a) Barborak, J. C.; Daub, J.; Follweiler, D. M.; Schleyer, P. v. R. *J. Am. Chem. Soc.* **1969**, *91*, 7760. (b) Barborak, J. C.; Schleyer, P. v. R. *J. Am. Chem. Soc.* **1970**, *92*, 3184.
(12) Grutzner, J. B.; Winstein, S. *J. Am. Chem. Soc.* **1970**, *92*, 3186; **1972**, *94*, 2200.
(13) Hoffmann, R.; Stohrer, W.-D.; Goldstein, M. J. *Bull. Chem. Soc. Jpn.* **1972**, *45*, 2513.
(14) (a) Goldstein, M. J.; Hoffmann, R. *J. Am. Chem. Soc.* **1971**, *93*, 6193. See also: (b) Goldstein, M. J. *J. Am. Chem. Soc.* **1967**, *89*, 6357. (c) Goldstein, M. J.; Odell, B. G. *J. Am. Chem. Soc.* **1967**, *89*, 6356.
(15) Yoneda, S.; Winstein, S.; Yoshida, Z. *Bull. Chem. Soc. Jpn.* **1972**, *45*, 2510.
(16) Huang, M. B.; Goscinski, O.; Jonsäll, G.; Ahlberg, P. *J. Chem. Soc., Perkin Trans. 2*, **1983**, 305.
(17) Huang, M. B.; Jonsäll, G. *Tetrahedron* **1985**, *41*, 6055.
(18) Jørgensen, K. A.; Linderberg, J.; Swanstrøm, P. *Collect. Czech. Chem. Commun.* **1988**, *53*, 2055.
(19) Bella, J.; Poblet, J. M.; Demoulliens, A.; Volatron, F. *J. Chem. Soc., Perkin Trans. 2*, **1989**, 37.
(20) Bouman, T. D.; Trindle, C. *Theor. Chim. Acta* **1975**, *37*, 217.

0002-7863/93/1515-7445$04.00/0

Scheme I

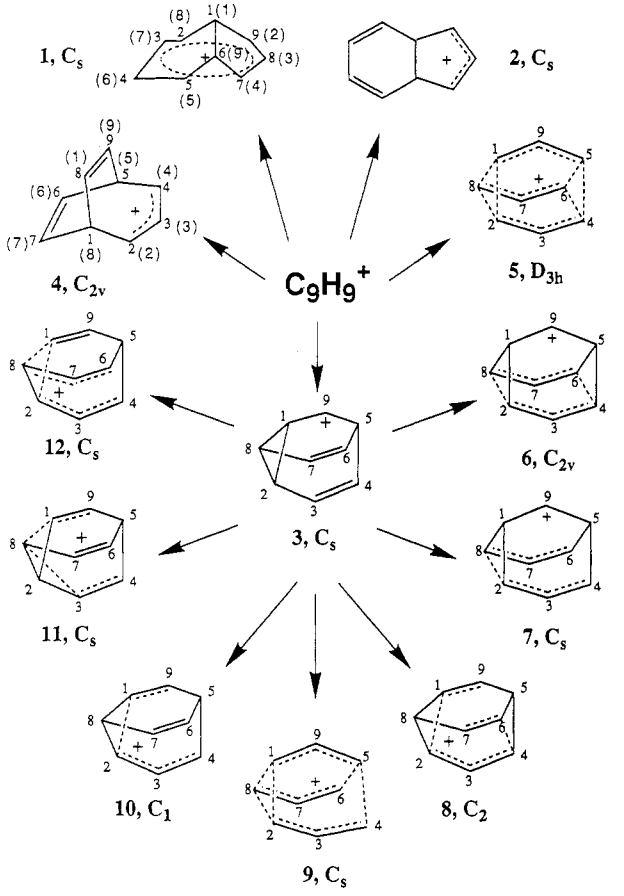

Scheme II

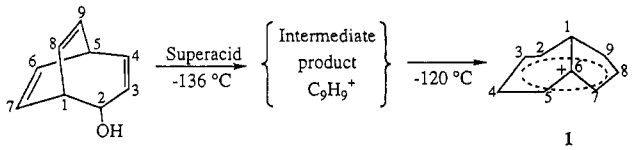

major pathway. The ^{13}C signal broadens and splits into two new signals at 101 and 152 ppm that can be assigned to groups of six and three equivalent C atoms, respectively. This is in line with a process such as A1 that according to Table I equilibrates C atoms 3, 7, and 9 (1, 2, 4, 5, 6, 8) (compare with Figure 1). Ahlberg and co-workers predicted that a process such as A should require an activation energy of ≤ 3.8 kcal/mol.[5-8]

2. Topology of the PES of the 9-Barbaralyl Cation (3)

The various rearrangement modes of **3** and the possible involvement of **4** and **5** either as TSs or intermediates have been the target of both experimental[5-12] and theoretical investigations.[13-20] The latter reach from orbital analysis,[13,14] early CNDO/2 calculations,[15] and MINDO/3, MNDO, and HF/STO-3G studies[16-19] to a recent HF/6-31G(d) investigation.[2] Special coordinates have been designed to follow the reaction path of the degenerate rearrangement of **3**,[18] and a permutation symmetry analysis has been performed to derive kinetic equations.[20] Even though these investigations mean a big step forward to the understanding of the degenerate rearrangements of **3**, no conclusion could be reached so far as for the relative stabilities of ions **1–5**, the preferred reaction paths of **3**, and the nature of TSs and possible intermediates. Therefore, a reliable ab initio investigation of the PES of **3** is highly desirable to get answers to these pending questions.

In Figure 1, possible rearrangements of **3** are schematically

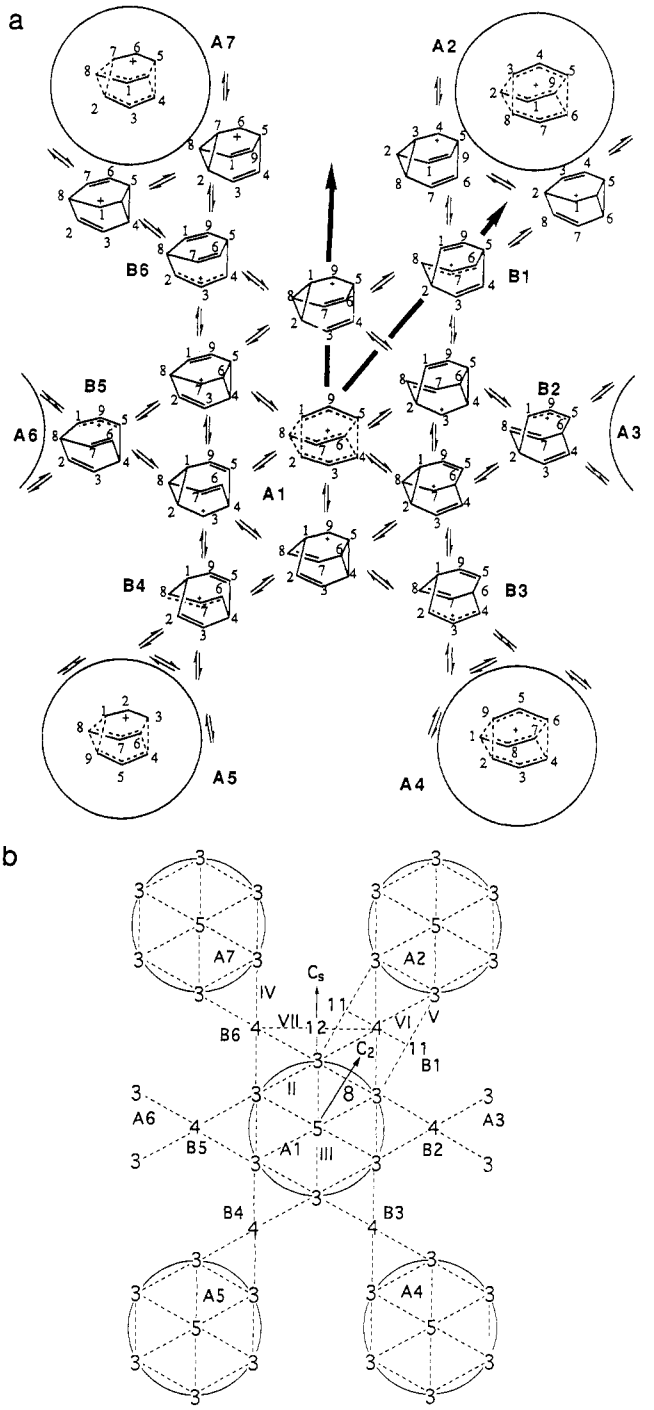

Figure 1. Schematic representation of the PES of $C_9H_9^+$ in the vicinity of the barbaralyl cation **3**. (a) Sixfold degenerate divinylcyclopropylcarbinyl rearrangements form cycle A1. Each of the six different forms of **3** of A1 are connected with the D_{3h} symmetrical ion **5** in the center of cycle A1. A1 itself is connected with six other rearrangement cycles A2–A7 via fourfold degenerate rearrangement processes B1–B6. Rearrangement cycles A2–A7 are characterized by the appropriate forms of **5** at the center of each cycle while B1–B6 are characterized by six different forms of ion **4**. The two arrows indicate the direction of the C_s and the C_2 search carried out in this work. Note that the directions A5–A1–A2, A4–A1–A7, and A3–A1–A6 are not in one plane because they are orthogonal to each other. (b) The diagram gives a connection between Figure 1a, the structures shown in Scheme I, and the reactions given in Scheme III. Each reaction path is indicated by a dashed line. Reaction paths V, VI, and VII are only given for the crossing from A1 to A2.

shown. Process A is a sixfold degenerate rearrangement that could involve very different TSs (see reactions I–III in Scheme

Table I. Equilibration of C Atoms of **3** by Processes A and B (see Figure 1)

cycle	equilibration of carbon atoms number[a]		cycles	equilibration of
A1	1,2,8,4,5,6	3,7,9	A1–B1–A2	all but 7
A2	2,3,8,5,6,9	1,4,7	A1–B2–A3	all but 9
A3	1,2,3,5,6,7	4,8,9	A1–B3–A4	all but 3
A4	1,2,9,4,6,7	3,5,8	A1–B4–A5	all but 7
A5	3,4,6,1,8,9	2,5,7	A1–B5–A6	all but 9
A6	1,7,8,3,4,5	2,6,9	A1–B6–A7	all but 3
A7	2,7,8,4,5,9	1,3,6	A2–B1–A1–B2–A3[b]	all
	no. of different forms if C atoms would be labeled[c]			
			3	181.440
			4	90.720
			5	30.240
			8	181.440
no. of A cycles				30.240
no. of B processes				90.720

[a] C atoms that equilibrate are given according to numbering in Figure 1. [b] Any similar combination of three A cycles leads to the same result. [c] Symmetry is considered in each case.

III). Since **3** possesses the divinylcyclopropane entity, one possibility is that **3** undergoes fast Cope rearrangements (see, reaction Ia in Scheme III) with a C_{2v} symmetrical TS **6** (Scheme I). Alternatively, structure **6** could be an intermediate being separated from **3** by C_s-symmetrical TSs **7** (see reaction Ib in Scheme III). However, in any case reaction I would connect only two structures on opposite sides of cycle A in Figure 1, and accordingly, it could not lead to a ^{13}C signal ratio of 6:3.

Alternatively, ion **5** could be the TS of the Cope rearrangement, as has been suggested by Hoffmann and co-workers[13] (see reaction IIIa in Scheme III). Since **5** is located in the center of cycle A, each of the six barbaralyl cation forms of cycle A (**3**, **3'**, **3''**, etc.) could be reached. This, however, would imply a threefold degenerate TS vector and a "monkey saddle" as a TS (six valleys meeting at TS **5**), which according to the McIver–Stanton symmetry rules for TSs[21,22] should not be allowed. Of course, a small perturbation of **5** could lead to a symmetry-allowed TS, so that reaction IIIa would not proceed exactly through **5** but for all practical purposes the energy of **5** would provide the activation energy of IIIa. Alternatively, structure **5** could be an intermediate being separated from **3** by TS **9** (reaction IIIb, Scheme III). Again, **5** would connect all structures **3** in cycle A, and therefore, reaction IIIb would lead to the observed NMR spectra at −151 °C. In this connection, the interesting questions would be whether **5** is stable enough to be detected and whether the geometries of **5** and **9** differ considerably.

A direct rearrangement of structure **3** to structures **3'**, **3''**, etc. along the periphery of cycle A requires a sequence of divinylcyclopropylcarbinyl cation–divinylcyclopropylcarbinyl cation rearrangements (type II reactions in Scheme III, see also Figure 1). In reaction II, one cyclopropane bond (e.g., C1–C2, Scheme III) is broken while at the same time another (e.g., C4–C6) is formed, thus leading to a delocalization of positive charge along a helically arranged sequence of bonds that connects the old C^+ center (e.g., C9) and the new one (e.g., C7). Hence, the TS possesses C_2 symmetry and corresponds to structure **8**. Type II reactions lead to the equilibration of C3, C7, and C9 (C1, C2, C4, C5, C6, C8) (see Table I) and, thereby, to the observed NMR signal intensities.

Various authors have discussed **4** as a transient structure of degenerate rearrangements of **3**.[5–20] Figure 1 shows that this is only possible if the molecule leaves cycle A, i.e. if rearrangement processes A and B take place at the same time, leading to complete scrambling of all nine CH groups of **3**. Process B can proceed either via reaction IVa, IVb, or V (Scheme III). In the first case,

(21) Stanton, R. E.; McIver, J. W., Jr. *J. Am. Chem. Soc.* **1975**, *97*, 3632.
(22) McIver, J. W., Jr. *Acc. Chem. Res.* **1974**, *7*, 72.

Scheme III

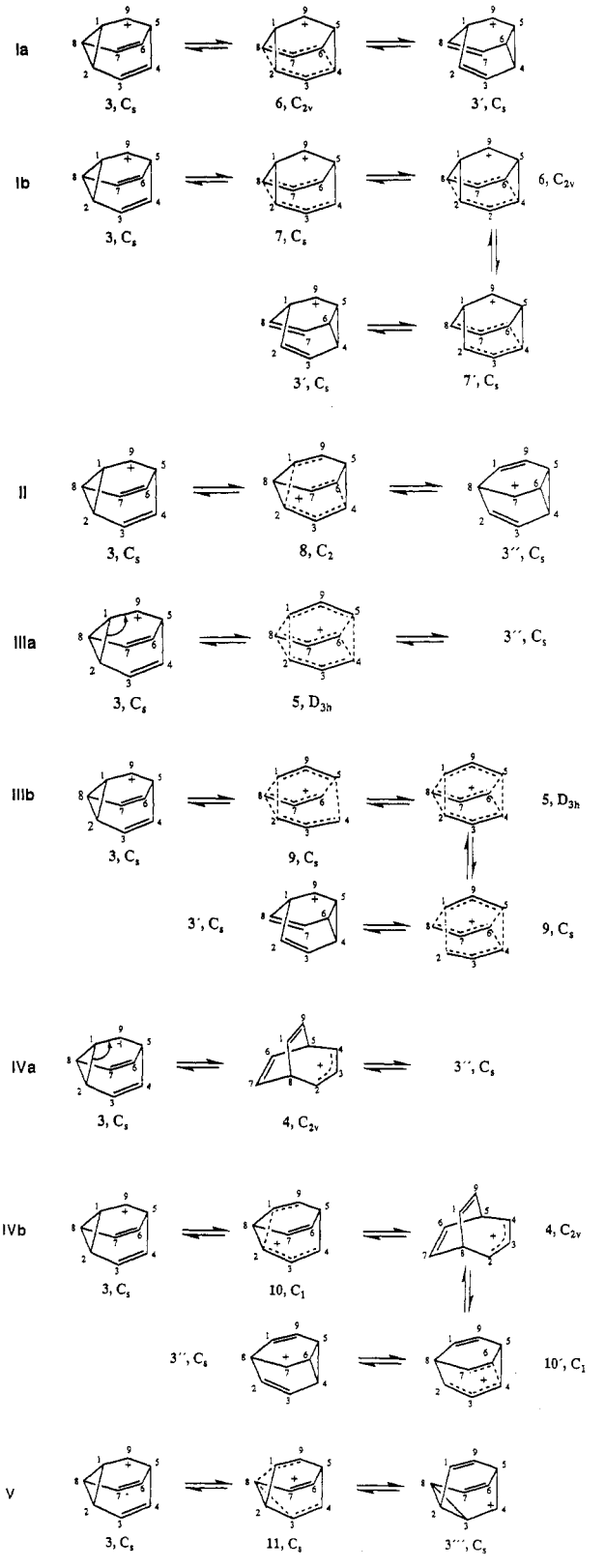

cation **4** functions as a TS; in the second case it functions as an intermediate, which is separated from **3** by TS **10** (Scheme I). Both possibilities are feasible, and none can be excluded on the basis of the available experimental results. If IVb dominates, again, the possibility of trapping **4** has to be considered. So far, there is no experimental evidence on the existence of a stable intermediate **4** although **4** is the logical primary product of reaction 1 (Scheme II).

Alternatively, **3** could jump from one A cycle to another by

Scheme IV

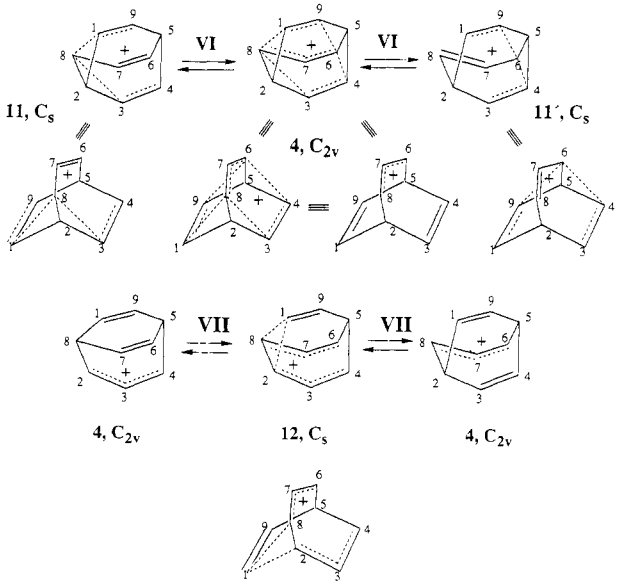

Table II. Possible Reaction Paths Leading to Degenerate Rearrangements of **3**

		characterization of transition state		
path	intermediate	structure	symmetry	TS allowed
Ia	no	**6**	C_{2v}	yes
Ib	**6**	**7**	C_s	yes
II	no	**8**	C_2	yes
IIIa	no	**5**	D_{3h}	no
IIIb	**5**	**9**	C_s	yes
IVa	no	**4**	C_{2v}	no
IVb	**4**	**10**	C_1	yes
V	no	**11**	C_s	yes
VI	no	**4**	C_{2v}	yes
VII	no	**12**	C_s	yes

reaction V, which involves TS **11** (Schemes I and III). In this way, completely degenerate rearrangements of **3** would not necessarily involve **4** as a transient point. As a matter of fact, with reaction V structure **4** would become a TS of higher order with more than one imaginary frequency, since two TSs **11** would be connected via path VI with **4** as a transient point (Scheme IV). Yet, another path (reaction VII in Scheme IV) is that leading directly from one structure **4**, e.g. at B1, to another, e.g. at B6, via structure **12** (Schemes I and IV).

In Table II, the possible reaction steps possibly being involved in degenerate rearrangements of **3** are listed and characterized according to the discussion given above. Figure 1b provides additional information by showing how the network of reaction paths I–VII leads to rearrangement cycles A1–A7 and the coupling processes B1–B6. Actually, Figure 1 gives only a small section of a complicated surface in four-dimensional space (the three directions A5–A1–A2, A4–A1–A7, and A3–A1–A6 are parallel to the three axes of an hypertorus, i.e. A2 and A7 (A2 and A3, etc.) are not directly connected via B processes) that hosts 30 240 different A cycles (leading to 181 440 different 9-barbaralyl cation forms[23]) and 90 720 different B processes (see Table I). As shown in Table I, a passage of **3** through just three different A cycles that do not lie on a line leads to an equilibration of all nine C atoms. However, passage through two A cycles connected by B processes leads to an equilibration of all C atoms but one. The energy barriers of reaction paths I–VII will determine the energetics of partially and completely degenerate rearrangements of **3**.

(23) These forms are different in the sense that if each C atom could be labeled by a number, each form would represent a different connectivity between the nine C atoms not considering symmetrically equivalent forms.

Here, we report for the first time extensive correlation-corrected ab initio (MP2 and MP4) calculations to describe reactions I–VII and degenerate rearrangements A and B in more detail. For this purpose, we have carried out geometry optimizations of most of the structures **1–12**. In addition, we have characterized stable $C_9H_9^+$ ions by calculating charge distribution and magnetic properties. This was done to get more information on CC bonding and charge delocalization in nonclassical C_9H_9 cations.

With this work we want to answer the following questions: (1) Which of the structures shown in Scheme I represent stable $C_9H_9^+$ ions, and which correspond to TSs on the PES? (2) Does the sixfold degenerate process A proceed via paths I, II, and/or III? What are the energy requirements of A? (3) Is structure **5** a (slightly distorted) TS or an intermediate of process A? Is there any possibility to experimentally detect **5**? (4) What is the reaction mechanism of the totally degenerate rearrangement of **3**? Does it involve structure **4** via reaction IV or does it circumvent **4** via reaction path V (see Figure 1a)? What are the energy barriers of the totally degenerate rearrangement of **3**? (5) Does structure **4** represent a stable species, or is it an experimentally not detectable transient point on the PES? (6) What are the electronic features of **3** that make it such a floppy cation? Do **3**, **4**, and **5** possess similar electronic features? (7) What are the magnetic properties of $C_9H_9^+$ ions **3**, **4**, and **5**, and how can they be related to their electronic features?

In the following we will investigate these questions. We start by describing computational methods used in this work (section 3). Then, we will present Hartree–Fock (HF) and Møller–Plesset perturbation theory (MP) descriptions of selected regions of the PES of $C_9H_9^+$. On the basis of these descriptions we will discuss reactions I–VII and processes A and B (section 4). Finally, in section 5, calculated magnetic properties will be compared with experimental values.

3. Computational Methods

In this work, we have used four different levels of theory. First we have carried out HF/6-31G(d) geometry optimizations[24] for structures **1–9** utilizing data we had previously obtained.[2] In the next step, we have repeated geometry optimizations at the MP2/6-31G(d) level[25] for some of the structures shown in Scheme I (**1–5**, **9**). Since this implied optimizations of up to 27 geometry parameters and since many of these parameters coupled, convergence could only be achieved by carefully selected starting geometries and frequent updates of the Hessian matrix by analytically calculated force constants from lower levels of theory.

For several structures, a corresponding stationary point cannot be found on the HF/6-31G(d) and/or MP2/6-31G(d) PES of $C_9H_9^+$ for reasons which will be discussed below. Therefore, we have explored the PES in a more systematic manner in the third step of the investigation. We have selected four directions that combine the locations of structures we want to investigate. Two of these PES searches are indicated in Figure 1. The first starts at structure **5** located at the origin of cycle A and follows reaction path III (Scheme III and Figure 1b) toward structure **3** and beyond **3** where it should lead to structure **12**. Since all $C_9H_9^+$ forms along this path possess at least C_s symmetry, we call this the C_s search.[26]

In the second search, we also start at **5** but follow now the direction that connects all structures with at least C_2 symmetry (C_2 search).[26] The C_2 direction lies between two type III reaction paths, crosses reaction path II at its midpoint, and then, leads to structure **4**. Because of symmetry reasons, the midpoint of II must be the location of TS **8**, and therefore, the C_2 search should lead to the detection of both **4** and **8**. In the third search, we have also started at **5** but performed it in a direction that leads to a C_{2v} distortion of **5** (C_{2v} search). This is the direction along which the Cope form **6** should be located. Finally, in the last search, we have

(24) Hariharan, P. C.; Pople, J. A. *Theor. Chim. Acta* **1973**, *28*, 213.
(25) Pople, J. A.; Binkley, J. S.; Seeger, R. *Int. J. Quantum Chem., Symp.* **1976**, *10*, 1.
(26) The actual driving parameter for the C_s search has been the distance $r(4,6)$, which means that the search direction is identical with that shown in Figure 1 only between **5** and **12**. Beyond **12** it differs from the C_s direction. The same applies to the C_2 search direction if one goes beyond **4**.

explored the PES in a direction that is perpendicular to that of the C_2 search but starts at **4** and leads to a possible TS **11** (**4–11** search).

In the C_s search we have carried out five MP2/6-31G(d), in the C_2 search eight, in the C_{2v} direction five, and in the **4–11** direction four HF/6-31G(d) geometry optimizations, using fixed values of distances C4–C6 ($r(4,6)$, C_s, C_2, and C_{2v} search) and C1–C8 ($r(1,8)$, **4–11** search). For all optimized geometries, we have carried out in the last step of the investigation single-point calculations at the MP3/6-31G(d), MP4(DQ)/6-31G(d), and MP4(SDQ)/6-31G(d) level of theory.[27]

Apart from the energy and geometry calculations, we have used the IGLO (individual gauge for localized orbitals) method by Kutzelnigg and Schindler[28] to calculate the magnetic properties of $C_9H_9^+$ cations. IGLO leads to reasonable ^{13}C NMR chemical shift values, and therefore, the method has been used by us[1,2] and others[29–31] to identify a given structure by comparison of theoretical and experimental chemical shift values. The shift values are sensitive to the geometry of the molecule in question, and this can be used, at least in a semiquantitative manner, for an alternative determination of the geometry. For example, Cremer and co-workers[1] have shown that the homoaromatic 1,7 distance of the homotropylium cation can be determined on the basis of a comparison of experimental and theoretical ^{13}C chemical shift values. In the same way, we have tried to get an independent determination of the geometry of **3** by computing IGLO chemical shift and magnetic susceptibility calculations for all structures along the C_s search direction.

Since structures **1–12** represent various degrees of bond delocalization and, therefore, cover the whole region from classical to nonclassical bonding, a detailed analysis of electron distribution and bonding in $C_9H_9^+$ cations was another goal of the present work. We have pursued this goal by investigating electron density distribution $\rho(r)$, Laplace concentration $-\nabla^2\rho(r)$, and energy density distribution $H(r)$ in the way described previously by two of us.[32,33] This analysis is based on the virial partitioning method of Bader and co-workers[34] and has helped to characterize bonding in many molecules with classical and nonclassical bonding situations.[35,36] In this work, we have used both HF/6-31G(d) electron densities and MP2/6-31G(d) response densities, where the latter have been calculated utilizing the method by Kraka and co-workers.[37,38]

Calculations have been performed on a CRAY XMP-416 using the COLOGNE90 ab initio package,[39] which includes an implementation of the IGLO method of Kutzelnigg and Schindler.[40] In addition, the GAUSSIAN90[41] and CADPAC ab initio packages[42] have been used.

Table III. Prediction of Stationary Points on the $C_9H_9^+$ PES

structure	HF[a]	MP2	MP3	MP4(SDQ)	prediction
1	no	yes	yes	yes	minimum
2	yes	no	no	no	no stationary point
3	yes	no	yes	yes	minimum
4	yes[b]	yes[b]	yes	yes	1st order TS
5	yes	yes	yes	yes	shallow minimum
6	no	no	no	no	no stationary point
7	no	no	no	no	no stationary point
8	no	no	yes	yes	1st order TS
9	no	no	yes	yes	1st order TS
10	not investigated				no stationary point
11	no	no	no	no	no stationary point
12	no	no	no	no	no stationary point

[a] Eigenvalues of Hessian matrix checked. Reference 2. [b] Minimum found within C_{2v} constraints.

4. Results and Discussion

Location and identification of the various $C_9H_9^+$ forms shown in Scheme I turned out to be extremely difficult, since both HF and MP2 failed to describe all forms in a consistent way. If one orders **1–12** according to the degree of bond delocalization that is reflected by their structure formulas from classical to nonclassical,

more classical → more nonclassical
2, 3, 4 **10, 8, 6, 7** **11, 1, 12, 9, 5**

then HF fails to describe the nonclassical structures while MP2 fails to describe the classical structures correctly. As a consequence, HF/6-31G(d) calculations lead to a local minimum corresponding to **2** but to no minimum corresponding to **1**.[3] In turn, the MP2/6-31G(d) PES of $C_9H_9^+$ contains stationary points corresponding to **1**, **4**, and **5** but not for **2** and **3** (compare with Table III) although the experimental evidence clearly suggests **3** to be a minimum structure.[5–8]

The failure of HF to correctly describe nonclassical structures, structures with bond delocalization, and those with stretched bonds has been often documented.[43] It has to do with the fact that HF largely overestimates the energy raise upon homolytic fission of a bond, which is a well-known artifact of the HF approach. MP2 and MP3 include double excitations that lead to electron pair correlation corrections. Accordingly, they can describe structures with stretched or dissolved bonds much better than HF. However, MP2 very often overestimates the stability of structures with stretched bonds, biradical nature, or delocalized bonds. Accordingly, MP2 leads to an artificial stabilization of nonclassical structures which can only be corrected if higher order correlation effects are included. The best way to do this would be by a coupled cluster method, but in view of the size of the $C_9H_9^+$ cations considered in this work, a computationally less demanding method must be used, for example MP4 with single (S), double

(27) Krishnan, R.; Pople, J. A. *Int. J. Quantum Chem.* **1978**, *14*, 91.
(28) (a) Kutzelnigg, W. *Isr. J. Chem.* **1980**, *19*, 193. (b) Schindler, M.; Kutzelnigg, W. *J. Chem. Phys.* **1982**, *76*, 1919.
(29) (a) Schindler, M. *J. Am. Chem. Soc.* **1987**, *109*, 1020. (b) Kutzelnigg, W.; Fleischer, U.; Schindler, M. *NMR, Basic Principles and Progress*; Springer Verlag: New York, 1991; Vol. 23, p 1.
(30) See, e.g.: (a) Hnyk, D.; Vajda, E.; Buehl, M.; Schleyer, P. v. R. *Inorg. Chem.* **1992**, *31*, 2464. (b) Buehl, M.; Schleyer, P. v. R. *J. Am. Chem. Soc.* **1992**, *114*, 477. (c) Buehl, M.; Schleyer, P. v. R.; McKee, M. L. *Heteroat. Chem.* **1991**, *2*, 499. (d) Buehl, M.; Schleyer, P. v. R. *Angew. Chem.* **1990**, *102*, 962. (e) Schleyer, P. v. R.; Buehl, M.; Fleischer, U.; Koch, W. *Inorg. Chem.* **1990**, *29*, 153. (f) Schleyer, P. v. R.; Koch, W.; Liu, B.; Fleischer, U. *J. Chem. Soc., Chem. Commun.* **1989**, 1098. (g) Bremer, M.; Schoetz, K.; Schleyer, P. v. R.; Fleischer, U.; Schindler, M.; Kutzelnigg, W.; Koch, W.; Pulay, P. *Angew. Chem.* **1989**, *101*, 1063.
(31) Buzek, P.; Schleyer, P. v. R.; Siebert, S. *Chem.-Ztg.* **1992**, *26*, 116 and references therein.
(32) (a) Cremer, D.; Kraka, E. *Angew. Chem., Int. Ed. Engl.* **1984**, *23*, 627. (b) Cremer, D.; Kraka, E. *Croat. Chem. Acta* **1984**, *57*, 1259.
(33) Kraka, E.; Cremer, D. In *Molecular Structure and Energetics, Structure and Reactivity*; Liebman, J. F., Greenberg, A., Eds.; VCH Publishers: New York, 1988; Vol. 7, p 65.
(34) (a) Bader, R. F. W.; Nguyen-Dang, T. T.; Tal, Y. *Rep. Prog. Phys.* **1981**, *44*, 893. (b) Bader, R. F. W.; Nguyen-Dang, T. T. *Adv. Quantum Chem.* **1981**, *14*, 63. (c) Bader, R. F. W. In *The Force Concept in Chemistry*; Deb, B. M., Ed.; Van Nostrand Reinhold Company: New York, 1981; p 39.
(35) (a) Cremer, D. In *Modelling of structure and properties of molecules*; Maksic, Z. B., Ed.; Ellis Horwood: Chichester, England, 1988; p 125. (b) Cremer, D.; Gauss, J.; Schleyer, P. v. R.; Budzelaar, P. H. M. *Angew. Chem., Int. Ed. Engl.* **1984**, *23*, 370. (c) Cremer, D.; Kraka, E. *J. Am. Chem. Soc.* **1985**, *107*, 3800, 3811. (d) Cremer, D.; Gauss, J. *J. Am. Chem. Soc.* **1986**, *108*, 7467. (e) Cremer, D.; Bock, C. W. *J. Am. Chem. Soc.* **1986**, *108*, 3375. (f) Koch, W.; Frenking, G.; Gauss, J.; Cremer, D.; Sawaryn, A.; Schleyer, P. v. R. *J. Am. Chem. Soc.* **1986**, *108*, 5732. (g) Koch, W.; Frenking, G.; Gauss, J.; Cremer, D. *J. Am. Chem. Soc.* **1986**, *108*, 5808. (h) Budzelaar, P. H. M.; Cremer, D.; Wallasch, M.; Würthwein, E.-U.; Schleyer, P. v. R. *J. Am. Chem. Soc.* **1987**, *109*, 6290. (i) Koch, W.; Frenking, G.; Gauss, J.; Cremer, D.; Collins, J. R. *J. Am. Chem. Soc.* **1987**, *109*, 5917. (j) Cremer, D.; Kraka, E. In *Molecular Structure and Energetics, Structure and Reactivity*; Liebman, J. F., Greenberg, A., Eds.; VCH Publishers: Deerfield Beach, FL, 1988; Vol. 7, p 65. (k) Cremer, D. *Tetrahedron* **1988**, *44*, 7427. (l) Cremer, D.; Gauss, J.; Kraka, E. *THEOCHEM* **1988**, *169*, 531. (m) Frenking, G.; Koch, W.; Reichel, F.; Cremer, D. *J. Am. Chem. Soc.* **1990**, *112*, 4240.
(36) Frenking, G.; Cremer, D. *Struct. Bonding (Berlin)* **1990**, *73*, 17.
(37) Kraka, E.; Gauss, J.; Cremer, D. *THEOCHEM* **1991**, *234*, 95.
(38) (a) Gauss, J.; Cremer, D. *Adv. Quantum Chem.* **1992**, *23*, 205. (b) Gauss, J.; Cremer, D. *Chem. Phys. Lett.* **1987**, *138*, 131. (c) Gauss, J.; Cremer, D. *Chem. Phys. Lett.* **1988**, *153*, 303.
(39) Gauss, J.; Kraka, E.; Reichel, F.; Cremer, D. *COLONGNE90*; University of Göteborg, Göteborg, Sweden, 1990.
(40) Kutzelnigg, W.; Schindler, M.; van Wüllen, G. *IGLO*; University of Bochum, Bochum, Sweden, 1989.
(41) Frisch, M. J.; Head-Gordon, M.; Trucks, G. W.; Foresman, J. B.; Schlegel, H. B.; Raghavachari, K.; Robb, M. A.; Binkley, J. S.; Gonzalez, C.; Defrees, D. J.; Fox, D. J.; Whiteside, R. A.; Seeger, R.; Melius, C. F.; Baker, J.; Martin, R. L.; Kahn, L. R.; Stewart, J. J. P.; Topiol, S.; Pople, J. A. *Gaussian 90*; Gaussian, Inc.: Pittsburgh, PA, 1990.
(42) Amos, R. D.; Rice, J. E. *CADPAC: The Cambridge Analytic Derivative Package*, 4.0 ed.; Cambridge University: Cambridge, U.K., 1987.
(43) See, e.g.: (a) Szabo, A.; Ostlund, N. S. *Modern Quantum Chemistry, Introduction to Advanced Electronic Structure Theory*; MacMillan: New York, 1982. (b) Hehre, W. J.; Radom, L.; Schleyer, P. v. R.; Pople, J. A. *Ab Initio Molecular Orbital Theory*; John Willey: New York, 1986. (c) See also ref 35.

Table IV. Ab Initio Geometries of Structures **3**, **4**, **5**, **8**, and **9** Calculated with the 6-31G(d) Basis[a]

parameter	3, C_s MP2	4, C_{2v} MP2	5, D_{3h} MP2	8, C_2 HF	9, C_s HF
r(1,2)	1.657	2.447	1.588	2.280	1.621
r(2,3)	1.459	1.390	1.400	1.378	1.411
r(3,4)	1.343	r(2,3)	r(2,3)	r(2,3)	1.382
r(4,5)	1.545	1.470	r(1,2)	1.486	1.556
r(5,6)	r(4,5)	1.540	r(1,2)	1.546	r(4,5)
r(6,7)	r(3,4)	1.327	r(2,3)	1.314	r(3,4)
r(7,8)	r(2,3)	r(5,6)	r(2,3)	1.516	r(2,3)
r(2,8)	1.458	r(4,5)	r(1,2)	r(4,5)	1.532
r(4,6)	2.400	r(1,2)	r(1,2)	r(1,2)	1.800
r(1,8)	r(1,2)	r(5,6)	r(1,2)	r(5,6)	r(1,2)
r(1,9)	1.357	r(6,7)	r(2,3)	r(6,7)	1.383
r(5,9)	1.476	r(5,6)	r(2,3)	r(7,8)	1.422
r(1,5)	2.441	2.456	2.405	2.435	2.406
r(3,7)	3.036	3.047	2.830	3.009	2.866
∠(1,2,3)	114.3	101.6	116.3	108.0	115.2
∠(1,2,8)	63.9	36.6	60.0	42.2	61.8
∠(1,8,2)	∠(1,2,8)	108.8	∠(1,2,8)	97.5	∠(1,2,8)
∠(1,8,7)	∠(1,2,3)	106.8	∠(1,2,3)	109.5	∠(1,2,3)
∠(1,9,5)	119.0	117.7	118.4	118.5	118.1
∠(2,1,8)	52.2	34.7	∠(1,2,8)	40.2	56.4
∠(2,1,9)	113.2	103.1	∠(1,2,3)	103.2	116.0
∠(2,3,4)	121.1	122.6	∠(1,9,5)	121.0	119.3
∠(2,8,7)	122.7	∠(1,8,2)	∠(1,2,3)	114.7	118.2
∠(3,2,8)	∠(2,8,7)	124.9	∠(1,2,3)	124.2	∠(2,8,7)
∠(3,4,5)	117.8	∠(3,2,8)	∠(1,2,3)	∠(3,2,8)	118.0
∠(3,4,6)	103.7	∠(1,2,3)	∠(1,2,3)	∠(1,2,3)	112.7
∠(4,5,6)	102.0	∠(1,8,2)	∠(1,2,8)	∠(1,8,2)	70.7
∠(4,5,9)	109.6	∠(1,8,2)	∠(1,2,3)	∠(2,8,7)	115.7
∠(4,6,5)	39.0	∠(2,1,8)	∠(1,2,8)	∠(2,1,8)	54.7
∠(5,6,7)	∠(3,4,5)	∠(1,9,5)	∠(1,2,3)	116.7	∠(3,4,5)

[a] Bond lengths in Å, angles in deg. Parameters that are identical because of symmetry are related to a previous entry in the table. For each geometry, the level of theory employed is indicated.

(D), and quadruple (Q) excitations (MP4(SDQ)).[27] By the S excitations, orbital relaxation effects and, by the Q excitations, pair,pair correlation effects are accounted for. Furthermore, the overestimation of the stability of structures with stretched bonds is corrected by a coupling between D excitations (MP3 effect) and between D and Q excitations.[27] Accordingly, we can expect that MP4(SDQ) helps to identify stationary points on the $C_9H_9^+$ PES and leads to a reasonable energy ordering of $C_9H_9^+$ forms.

Although methods and programs (COLOGNE90[39]) are available to do MP4 geometry optimizations with analytical gradients,[38] the size of the ions investigated prevented these calculations. Nevertheless, useful MP4(SDQ) results have been obtained from single-point calculations at HF and MP2 optimized geometries located along the C_s, C_2, C_{2v}, and **4**–**11** search directions. These calculations are the basis for the ab initio description presented in the following, and the predictions given in Table III.

Calculated geometries and energies are summarized in Tables IV and V. Figures 2, 3, and 4 display sections of the $C_9H_9^+$ PES along the C_s, C_2, and C_{2v} directions.

9-Barbaralyl Cation (3). No minimum corresponding to **3** could be found at the MP2/6-31G(d) level (see Figure 2). The MP2 PES in the C_s direction only shows an inflection point for a r(4,9) distance close to 2.3 Å. However, **3** is a minimum structure at the HF/6-31G(d), MP3/6-31G(d), and MP4(SDQ)/6-31G(d) levels of theory (see Figure 2). MP4(SDQ) predicts a minimum about 7 kcal/mol below **5** at r(4,9) = 2.4 Å. Results of the MP2/6-31G(d) optimization at this r(4,9) value are listed in Table IV and are compared with the corresponding HF parameters in Figure 5. Figure 5 reveals that the two geometries are surprisingly close to each other. With a few exceptions, the MP2 values of the CC single bonds are slightly shorter while the CC double bonds (including the three-membered ring bonds) are slightly longer than the corresponding HF values. Hence, bond delocalization is somewhat larger at the MP2 level. Apart from this there are hardly any significant changes between the MP2 and HF geometries of **3**.

Table V. Absolute and Relative Energies of Structures **1**–**9** Obtained with a 6-31G(d) Basis[a]

structure	HF	MP2	MP3	MP4(DQ)	MP4(SDQ)
3	−345.72583	−346.90881	−346.90471	−346.90419	−346.91776
1		−15.7	−8.7	−7.8	−8.3
2	−16.7	−2.4	−6.5	−6.2	−6.7
3	0	0	0	0	0
4	−0.1	9.1 (8.3)	5.7 (5.6)	5.5 (5.5)	4.6 (4.7)
5	20.7	−8.4 (−9.6)	4.9 (4.8)	5.7 (5.6)	6.9 (6.7)
8	1.3	4.8	4.2	4.4	3.6
9		−5.8	6.4	7.1	8.1

[a] Absolute energies in hartree, relative energies in kcal/mol. MP3 and MP4 energies have been obtained for frozen cores. All MP energies with the exception of those for **8** have been calculated for MP2/6-31G(d) optimized geometries. Values in parentheses have been calculated for HF/6-31G(d) optimized geometries of **3**, **4**, and **5**. This holds also for the energies of **8**.

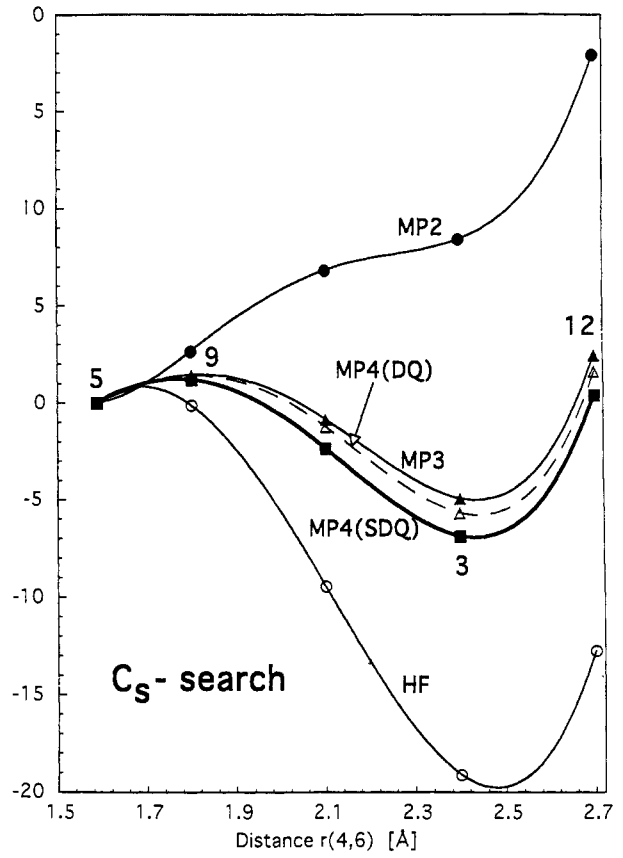

Figure 2. PES of $C_9H_9^+$ in the C_s direction indicated in Figure 1.

The striking feature of the geometry of **3** is the cyclopropylcarbinyl cation entity (C1C2C8C9) with its long, labile distal CC bonds (r(1,2) = 1.657 Å), the shortened basal bond (r(2,8) = 1.458 Å), and the short exocyclic C1C9 bond (r(1,9) = 1.357 Å, Table IV, Figure 5). Calculated geometrical parameters are close to those found for the cyclopropylcarbinyl cation (**13**) itself,[44] which suggests that **3** shows the same enhanced reactivity as **13**. In particular, the three-membered ring bonds of **3**, which possess bond orders of just 0.54[45] (Figure 6), will easily open, leading to a large reorganization of electron density and bonding. Cremer and co-workers[44] have studied this process in detail for **13** utilizing the topological analysis of $\rho(r)$. A similar analysis for **3** also shows the lability of the distal CC bonds, which at their bond

(44) Cremer, D.; Kraka, E.; Slee, T. S.; Bader, R. F. W.; Lau, C. D. H.; Nguyen-Dang, T. T. *J. Am. Chem. Soc.* **1983**, *105*, 5069.

(45) Bond orders n have been calculated from the equation $n = \exp[A(\rho(r_B) - B)]$, where $\rho(r_B)$ denotes the electron density at the bond critical point r_B and constants A and B have been determined from MP2/6-31G(d) response densities at the CC bond critical points of ethane and ethylene. See ref 33.

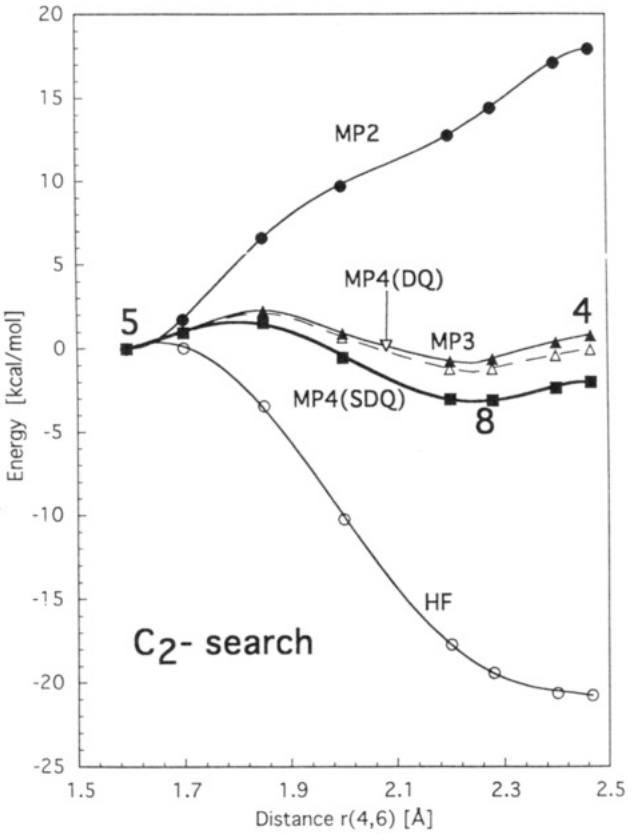

Figure 3. PES of $C_9H_9^+$ in the C_2 direction indicated in Figure 1.

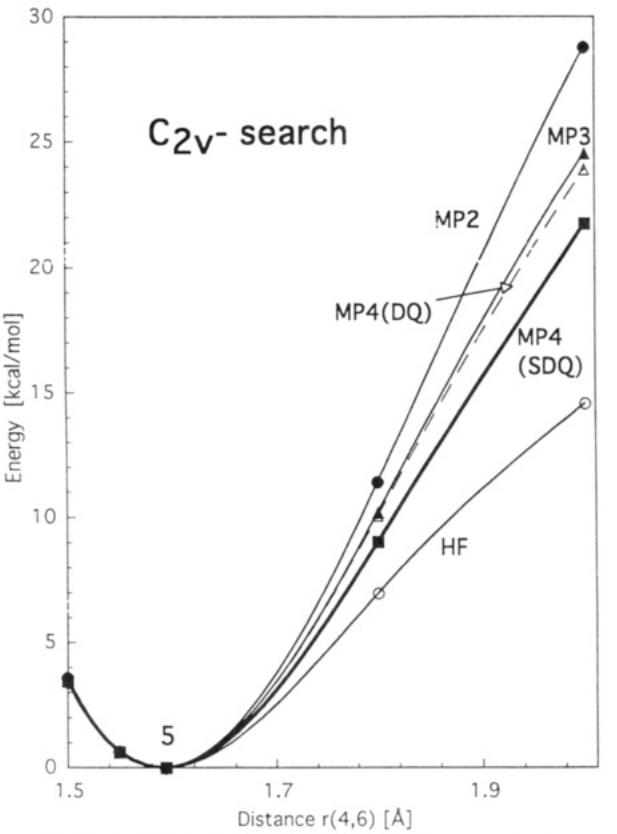

Figure 4. PES of $C_9H_9^+$ in the C_{2v} direction which connects structure **5** with possible Cope structures **6**.

critical point have an electron density only slightly larger than that at the ring critical point. There is a trough in the distribution of charge in the plane of the ring linking these three critical points, and little energy is required to break any of the two CC

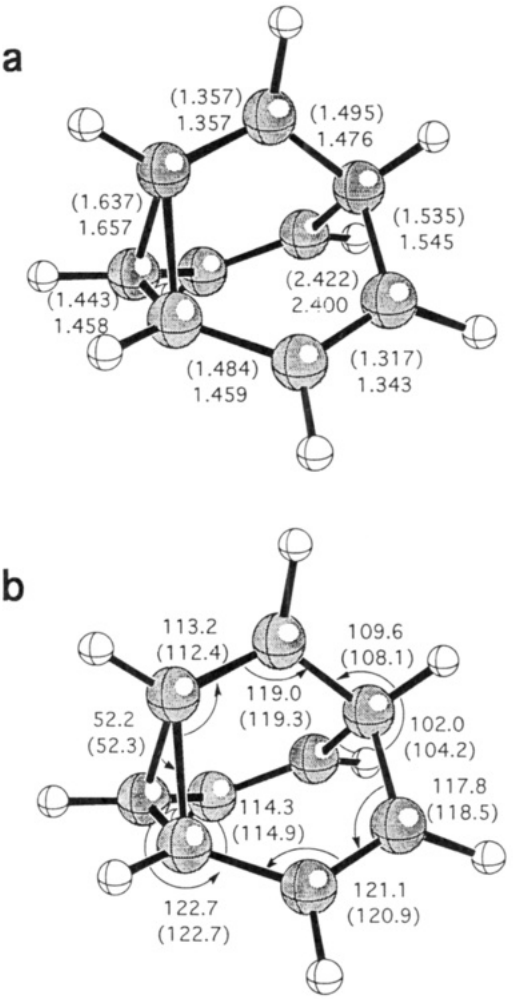

Figure 5. (a) and (b) MP2/6-31G(d) geometry of the barbaralyl cation **3** obtained at a MP4(SDQ)/6-31G(d) optimized $r(4,6)$ distance (see text). Numbers in parentheses give the HF/6-31G(d) optimized geometry of **3**.

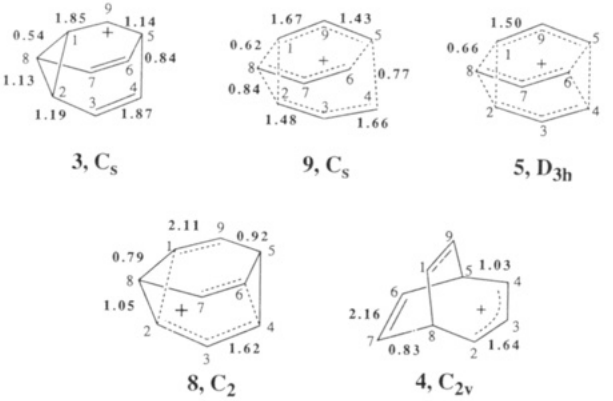

Figure 6. MP2/6-31G(d) bond orders of **3**, **9**, **5**, **8**, and **4**.[45]

bonds and to lead to an opening of the three-membered ring. This is nicely reflected by a perspective drawing of the MP2/6-31G(d) Laplace concentration of electrons, $-\nabla^2\rho(r)$ shown in the plane of atoms C1C2C8 (Figure 7). The strongest concentration of electrons is in the C2–C8 bond while in the region of bonds C1–C2 and C1–C8 concentration is weak and similar to that inside the three-membered ring.

Reaction Path II and Transition State 8. One of the distal bonds C1–C2 and C1–C8 will be broken if **3** rearranges via reaction path II and TS **8**. HF and MP2 searches for TS **8** were not successful. Therefore, we have used the fact that if TS **8** does exist, it must correspond to a minimum along the C_2 search

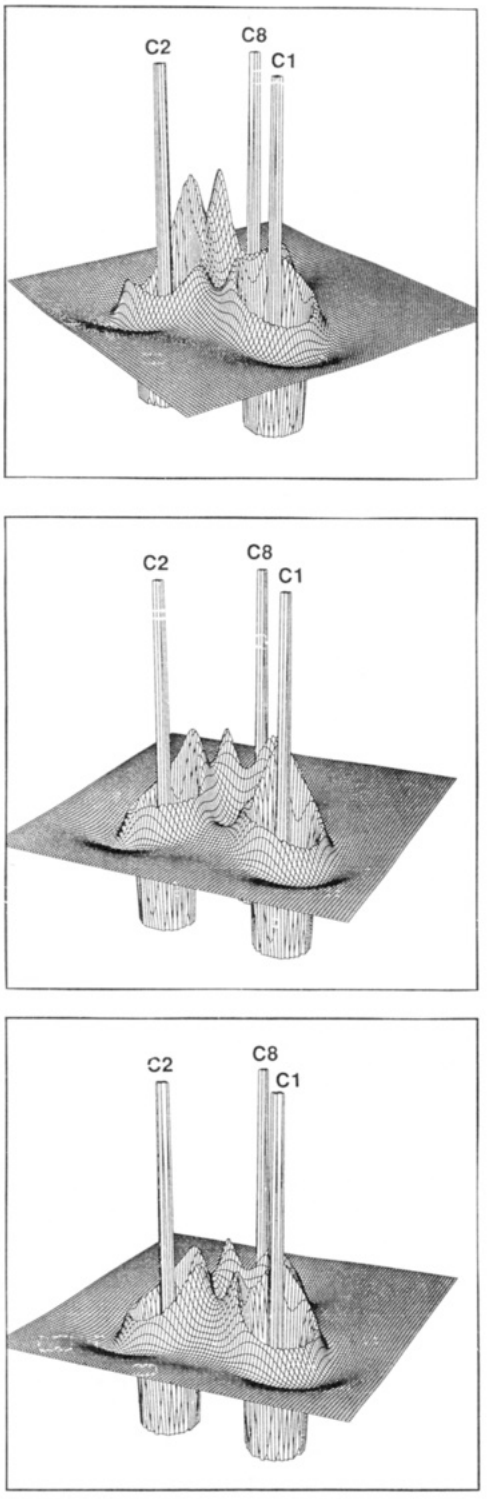

Figure 7. Perspective drawings of the MP2/6-31G(d) Laplace concentration $-\nabla^2\rho(r)$ calculated for the plane containing atoms C1, C2, and C8 of (a, top) **3**, (b, middle) **9**, and (c, bottom) **5**.

direction located between structures **5** and **4** (compare with Figure 1). Indeed, both the MP3 and the MP4(SDQ) PES in the C_2 direction possess a shallow minimum at about $r(4,6) = 2.28$ Å (compare with Figure 3). This point corresponds to a maximum along reaction path II and, therefore, is identical with TS **8**. According to MP4(SDQ)/6-31G(d) calculations carried out at the HF/6-31G(d) geometry for $r(4,6) = 2.28$ Å, TS **8** is just 3.6 kcal/mol above the energy of **3**, which means that the calculated activation energy of reaction II is very close to the experimental estimate for the activation barrier of process A (3.8 kcal/mol[5-8]).

The geometry of TS **8** is given in Table IV, and the calculated MP2/6-31G(d) bond orders are given in Figure 6. It confirms that a relatively small increase in energy leads to a drastic change in the geometry of **3**. One of the labile three-membered ring bonds opens from 1.66 to 2.28 Å while the other shortens to 1.55 Å. At the same the distance $r(4,6)$ decreases from about 2.40 to 2.28 Å and the positive charge is delocalized from C9 via C1, C8, C7, C6, and C4 to C3. These changes indicate that the cyclopropylcarbinyl cation entity is replaced by two homoallyl cation units. The electron density analysis shows that despite the large change in geometry the actual change in the electronic structure is relatively small, which is in line with the observations made for the opening of **13** to an homoallyl cation.[44]

The geometry (Table IV) and calculated bond orders of **8** (Figure 6) clearly show that this form is actually very close to that of ion **4**, which possesses similar geometrical parameters and bond orders. This can be rationalized by redrawing **8** in the way **4** is drawn and by considering the fact that **4** is the next neighbor of TS **8** on the PES (Figure 1).

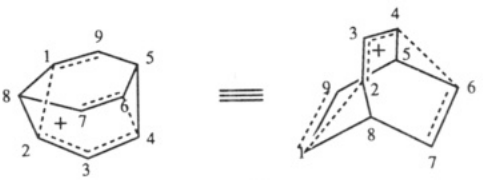

8, C_2

Reaction Path III and the Role of the D_{3h}-Symmetrical Ion 5. As has been pointed out in the introduction, the available experimental evidence does not exclude structures **5** and **6** as transient forms of the sixfold degenerate rearrangement A. To reach these forms the more stable C2–C8 bond (bond order 1.13, Figure 6) of the cyclopropylcarbinyl cation unit of **3** has to be weakened. This should require more energy than an opening of labile bonds C1–C2 and C1–C8. Of course, a synchronous shortening of distance C4–C6 or a synchronous opening of bonds C1–C2 and C1–C8 may make this process energetically favorable.

Structure **5** can be reached by following reaction path III, which is parallel to the C_s search direction (Scheme III and Figure 1). Figure 2 and the relative energies in Table V reveal that **5** lies about 7 kcal/mol above **3**, from which it is separated by a maximum of about 8 kcal/mol along the C_s direction. The maximum is the location of TS **9** ($r(4,6) = 1.80$ Å), which means that, according to MP3 and MP4(SDQ) theory, path IIIb rather than IIIa connects **3** with **5** and that **5** is an intermediate rather than a TS.

As noted in Section 2, the possibility of ion **5** being a TS (reaction IIIa) can be excluded according to the McIver–Stanton symmetry rules for TSs.[21,22] While it is not surprising that our calculations confirm this prediction, it is interesting to see that our results also exclude slightly distorted forms of **5** as possible TSs. The geometry and electronic structure of TS **9** are clearly different from those of **5** (Table IV and Figure 6). It seems that the symmetry requirements for TSs imply a stronger distortion of **5** than that caused by a small vibrational motion that lowers its D_{3h} symmetry to C_s. Of course, the energy difference between **5** and **9** is (with 1 kcal/mol) rather small, and therefore, it is highly unlikely to experimentally detect **5**.

Because of its symmetry **5** possesses just two types of bonds, namely elongated three-membered-ring bonds (1.588 Å, Table IV) and bridge bonds, that with lengths of 1.400 Å remind one of an aromatic system. Calculated MP2/6-31G(d) bond orders (Figure 7) show that it is more reasonable to consider **5** as being made up of three allyl cation units (with a positive charge of 0.33 e) weakly kept together by four-electron three-center bonds. This is revealed by bond orders of 1.50 for the bridge bonds, suggesting for each allyl cation unit 2π electrons and bond orders of 0.66 for the three-membered-ring bonds. For such a system, Goldstein and co-workers[14] have predicted anti-bicyloaromaticity, which

Scheme V

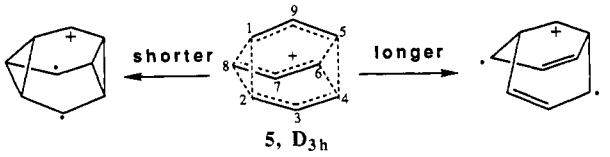

5, D_{3h}

would explain the lower stability of **5** as compared with that of **3**. However, the concept of bicycloaromaticity has recently been questioned,[46] and therefore, it might be more reasonable to point out that the stability of **5** suffers from the fact that only four electron pairs are available for six three-membered-ring bonds.

From an electronic point of view, reaction IIIb can be best understood as a shift of one electron (see bond orders in Figure 6) from the three-membered-ring end of **3** to the opposite end. This leads to an unfavorable buildup of negative charge in the bridges of TS **9** (0.8 e, see Figure 6), which may cause the energy increase of 8 kcal/mol. According to the analysis of $\rho(r)$ and the Laplace concentration $-\nabla^2\rho(r)$ (compare with Figure 7), TS **9** is close to the point at which the C4–C6 bond is formed on the way to **5**.

Reaction Path I (Cope Path). In Figure 4, the PES is given along the C_{2v} search direction, which leads from **5** to possible Cope structures such as **6**. These forms can be found by fixing bond lengths C2–C8 and C4–C6 to either longer or shorter values than those obtained for **5** and, then, reoptimizing all other geometrical parameters within C_{2v} symmetry. We have checked both possibilities, the results of which are summarized in Figure 4. Both lengthening and shortening of bonds C2–C8 and C4–C6 leads to an increase in energy. This could be due to the fact that both distortion modes must lead to unstable forms with high biradical character (Scheme V).

In any case, the results shown in Figure 4 exclude Cope structure **6** as an intermediate of reaction I and, thereby, also TS **7** (Scheme III). In order to exclude **6** also as a possible TS, we have carried out TS searches along the C_{2v} direction. None of these searches gave any indication of a C_{2v} symmetrical TS **6**, and therefore, we feel safe to say that **6** does not correspond to a stationary point on the $C_9H_9^+$ PES and that neither reaction Ia nor Ib corresponds to a minimum-energy path on the PES. However, substituents can make reaction path I energetically favorable, as has been demonstrated experimentally.[9]

Reaction Path IV and the Role of the Bicyclo[3.2.2]nona-3,6,8-trien-2-yl Cation (4). HF and MP2 geometry optimizations of **4** under C_{2v} symmetry constraints lead to a minimum, which, in the HF case, has been characterized by the eigenvalues of the corresponding Hessian matrix. Structure **4** can also be reached by extending the C_2 search beyond the location of TS **8**. Figure 1 reveals that the PES in the C_2 direction is symmetric with regard to **4**, i.e. **4** must correspond either to a minimum or a maximum in this direction. As shown in Figure 3, MP2, MP3, and MP4(SDQ) predict that **4** is actually a maximum rather than a minimum in the C_2 direction. *Obviously, we encounter with 4 one of these cases where symmetry constraints lead to erroneous predictions as to the nature of a stationary point on the PES.*[47]

Actually, the fact that **4** corresponds to a maximum rather than a minimum in the C_2 direction is not surprising in view of the experimental results.[5-8] If **4** would correspond to a minimum in the C_2 direction, this would imply that its relative energy is lower than that of **8** and that **4** is the TS of both processes A and B. Accordingly, one should find for **3** even at −151 °C one signal in the ^{13}C NMR spectrum resulting from completely degenerate

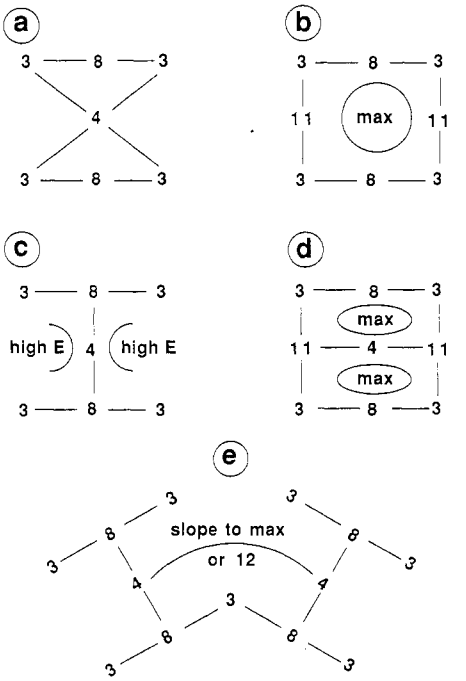

Figure 8. Schematic representation of possible reaction mechanisms for process B (see text). (a) Fourfold degenerate rearrangement with **4** as a TS or intermediate. (b) Twofold degenerate rearrangement via TS **11**. (c) Double-bifurcation mechanism via TSs **8** and **4**. (d) Double-bifurcation mechanism via TSs **11** and **4**. (e) Super-bifurcation mechanism connecting two processes B. Reaction paths are given by solid lines, stationary points by appropriate structure numbers (compare with Scheme I). A maximum (max) of energy or a high-energy (high E) region is indicated.

rearrangements. However, in view of the experimental results, this possibility can be excluded. Of course, **4** could also correspond to a shallow minimum even though its energy is higher than that of **8**. But we can also exclude this possibility on the basis of exploratory calculations in the immediate vicinity of **4**, which give no indication of a shallow minimum at the location of **4**.

How does the fact that **4** corresponds to a maximum in the C_2 direction comply with or contradict a possible reaction path IV? To answer this question, in Figure 8 four possible B mechanisms (a–d) are schematically outlined. If process B proceeds via reaction IV, then mechanism a of Figure 8 will apply. But mechanism a is not possible because of two reasons. First, McIver–Stanton symmetry rules for TSs[21,22] require that reaction IVa with a TS **4** is not possible and that mechanism a could only be based on reaction IVb. Reaction IVb, however, implies a TS **10** with a relative energy higher than that of **4**. Since our calculations describe **4** as a maximum in the C_2 direction, there must be a mechanism c that connects TS **8** in one A cycle with another TS **8** in another A cycle via a TS **4** (Figure 8) and that is energetically more favorable than mechanism a following reaction path IVb. Therefore, we can exclude mechanism a and refrain from a computational search for TS **10** on the PES.

A possible mechanism c is peculiar in the way that it involves a sequence of three first-order TSs in process B. TS **4** at the center is connected with two TSs **8**, at both of which the reaction path can branch in two directions thus connecting four different forms of **3**. Hence, mechanism c is best described as a double-bifurcation mechanism leading to a fourfold degenerate rearrangement of **3**. Alternatively, B could proceed via mechanism b in Figure 8, which involves reaction path V and TS **11**. Within mechanism b, ion **4** would correspond to a maximum (or higher order TS), which is in line with our calculational results. However, a combination of reaction paths V and VI to yield the double-bifurcation mechanism d (Figure 8) can be excluded, since it implies **4** to be a (shallow) minimum in the C_2 direction (see above).

(46) Schötz, K.; Clark, T.; Schleyer, P. v. R. *J. Am. Chem. Soc.* **1988**, *110*, 1394.

(47) Of course, such an error could be avoided by calculating the eigenvalues of the Hessian matrix at this point. However, second-derivative calculations at the MP2/6-31G(d) level were not feasible for $C_9H_9^+$.

It is difficult to predict whether a TS **4** or a TS **11** should be energetically more favorable. A potential TS **11** can be best visualized by realizing that **3** contains a 2-vinyl–cyclopropylcarbinyl cation unit that can undergo a degenerate bishomoallyl cation rearrangement leading to a new form of **3** located in a new A cycle. Since such a rearrangement could not be excluded on the basis of the experimental and calculational results, we have answered the question whether b or c is the correct mechanism for process B by carrying out a PES search in the **4**–**11** direction along reaction path VI (compare with Scheme IV). This has been done by stepwise decreases of distances C1–C8 and C3–C8 from their value in **4** (2.467 Å, Table IV) to 2.20 Å and reoptimization all other parameters. At all levels of theory considered, the relative energy steadily increased and reached 15 kcal/mol at 2.20 Å (MP4(SDQ) results). Clearly, these results exclude mechanism b in Figure 8 and, thereby, any reaction path (V and VI) that would involve a first order TS **11**.

Our analysis of process B leads to the double-bifurcation mechanism c as the energetically most favorable one. In the literature, one has speculated about bifurcation mechanisms in connection with, e.g., the olefin metathesis reaction or electrocyclic reactions,[21,48] but no direct experimental or calculational evidence has been given so far. To our knowledge, the degenerate rearrangement of **3** is the first example for which a double-bifurcation mechanism is described in detail. We have also investigated the possibility that two double-bifurcation steps are connected by a third bifurcation mode involving a first-order TS **12** and reaction path VII (Scheme IV and Figure 8e). Since **12** would be located in the C_s direction somewhere outside cycle A, we have extended the C_s search to this region. But no further stationary point has been found, and therefore, we exclude a TS **12** and any higher bifurcation mechanism such as the one shown in Figure 8e.

Since TS **4** possesses the highest energy (4.6 kcal/mol, MP4(SDQ)/6-31G(d), Table V) along reaction path c, its energy corresponds to the activation energy of process B. B connects different A cycles (Figure 1), and the combination of at least three A cycles by two B processes (see Table I) leads to a totally degenerate rearrangement of **3**. Accordingly, it is reasonable to compare the experimental activation energy (5.0 kcal/mol) for completely degenerate rearrangements of **3** with a calculated activation energy of 4.6 kcal/mol. The agreement is satisfactory and gives further support to the double-bifurcation mechanism c (Figure 8).

Our finding that **4** corresponds to a TS rather than a minimum-energy structure and, thereby, cannot be detected by experimental measurements is novel but not in contradiction with experimental investigations, which so far have not given evidence for the existence of **4**. This, of course, does not exclude the possibility that cation **4** can be generated in the form of a tight ion pair in a solvolysis reaction.[11] However, if **4** participates in an ion pair, then its charge distribution will probably differ considerably from that calculated in this work, and therefore, it should be appropriate to distinguish between **4** and the solvolysis intermediate.

Goldstein and co-workers[14] have predicted **4** to be destabilized by anti-bicycloaromatic interactions involving 6π electrons. MP2/6-31G(d) bond orders of **4** (Figure 6) suggest that actually 7.2 π-electrons (total π-bond order in **4**, $2(2.16) + 2(1.64) - 4 = 3.6$; number of π-electrons, $2(3.6) = 7.2$) are involved in these interactions, and accordingly, **4** should be less stable than **5**, which contains a bicyclic 6π ensemble (Figure 6). Obviously, anti-bicycloaromaticity, if it really exists, may be just one factor that besides strain effects, hyperconjugation, homoconjugation, and bond weakening by bond delocalization determines the stability of **4** and **5**. Apart from this it is interesting to note the close relationship between TSs **4** and **8** as it is reflected by their relative energies (Table V), calculated geometries (Table IV), charge distributions, and the bond orders shown in Figure 6. Also, the electronic structures of **3** and **4** are similar, as is reflected by calculated bond orders (Figure 6). Four of the six formal single bonds of **4** have the same bond order (0.83) as bonds C4–C5 and C5–C6 of **3**. There is a buildup of electron density in the nonbonding region between C1, C2 (C4, C9) and C8 (C5) that is similar to that calculated between atoms C4 and C6 of **3**. Hence, the computed electron density distribution clearly indicates its labile CC bonds, the rearrangement possibilities of **4**, and the relationship between structures **3**, **8**, and **4**.

(48) Basilevsky, M. V. *Chem. Phys.* **1982**, *67*, 337.

Table VI. Magnetic Properties of Ions **3**, **4**, and **5** Calculated at the IGLO/6-31G(d) Level of Theory[a]

parameter	**3** MP4-MP2[b]	**4** MP2[b]	**5** MP2[b]
δ(C1)	82.7	147.5	69.3
δ(C2)	91.4	235.5	δ(C1)
δ(C3)	125.2	135.7	144.3
δ(C4)	140.3	δ(C2)	δ(C1)
δ(C5)	51.1	55.0	δ(C1)
δ(C9)	249.2	δ(C1)	δ(C3)
$-\chi$	85.9	71.9	115.9

[a] Chemical shifts δ(C) in ppm relative to $(CH_3)_4Si$; magnetic susceptibility $-\chi$ in 10^{-6} cm^3 mol^{-1}. For numbering of atoms, see Scheme I. [b] Geometry calculated at the MP*n*/6-31G(d) level of theory.

5. Structure Determination by NMR Chemical Shift Calculations

In Table VI, IGLO/6-31G(d)//MP2/6-31G(d) ^{13}C chemical shifts and magnetic susceptibilities of cations **3**, **4**, and **5** are listed. As has been discussed various times in the literature,[1,2,28–31] chemical shift values depend critically on the geometry, and therefore, a comparison of calculated and experimental chemical shifts can be used for an alternative determination of molecular structure.

Unfortunately, the detailed ^{13}C NMR spectrum of **3** has not been measured so far. What is known[5–8] is the spectrum of the rearranging ion **3** at −151 °C, in which atoms C3, C7, and C9 (formally carrying the positive charge) and atoms C1, C2, C4, C5, C6, and C8, respectively, are equilibrated, thus leading to the observed intensity ratio of 3:6. Ahlberg and co-workers[7] have suggested experimentally based estimates for the ^{13}C chemical shift values of **3** derived from 9-methyl-**3** using appropriate shift corrections for the methyl group. Recently, we have shown that these estimates lead to reasonable reference data, provided shift values for C2, C8, and C9 are excluded from the set.[2] In the cyclopropylcarbinyl cation unit of **3**, the empty $2p\pi$ orbital at C9 overlaps with the antibonding C2–C8 Walsh orbital and withdraws electronic charge from the latter, thereby increasing the stability of the bond C2–C8. A methyl substituent at C9 changes the electron acceptor ability of the $2p\pi$ orbital and, accordingly, changes charges and shift values at C2, C8, and C9 in a way that is difficult to cover by increment values.

Table VII gives time-averaged ^{13}C chemical shift values for cations **3**, **4**, and **5**, where for each structure C atoms are grouped in a way that could lead to the observed 3:6 intensity ratio as a result of symmetry or because of some rapid degenerate rearrangements. Also shown are time-averaged ^{13}C chemical shifts for a completely degenerate rearrangement of the barbaralyl cation. In view of the C_{2v} symmetry of **4**, there are two formal possibilities to group C atoms in a 3:6 ratio, but none of these leads to time-averaged shift values close to those observed experimentally (see Table VII). The time-averaged ^{13}C shift values of both **4** and **5** differ by ≥24 ppm from the experimental values, which is far outside the accuracy of ^{13}C shift values (about 7 ppm[1]) that can be achieved at the IGLO/6-31G(d)//MP2/6-31G(d) level of theory. This accuracy is only reached with the shift values of **3** utilizing its MP4(SDQ)-MP2/6-31G(d) geometry (Figure 5 and Table IV).

Table VII. Time-Averaged ^{13}C Chemical Shifts of Cations **3**, **4**, and **5**

cation	geometry	centers	δ (ppm)	centers	δ (ppm)	mean deviation Δ[b]
3	MP2	3, 7, 9	167	1, 2, 4, 5, 6, 8	99	6
	HF		169		96	9
	MP2	all	122			4
	HF		121			3
4	HF	2, 3, 4	203	1, 5, 6, 7, 8, 9	114	26
	MP2		202		117	27
	HF	1, 3, 5	81	2, 4, 6, 7, 8, 9	175	73
	MP2		82		177	74
	HF	all	144			26
	MP2		145			27
5	HF	3, 7, 9	107	1, 2, 4, 5, 6, 8	182	69
	MP2		144		69	24
	HF	all	157			39
	MP2		94			24
expt[a]	process A		152		101	
	process A + B		118			

[a] Process B takes place at −135 °C and higher temperatures while process A already takes place at −152 °C (see ref 9). [b] The mean deviation Δ has been calculated using experimental shift data from ref 6.

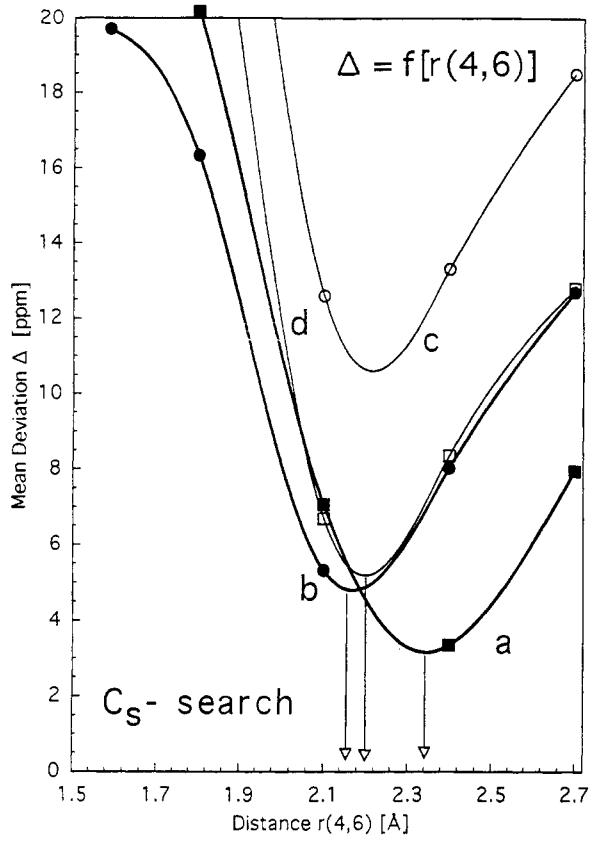

Figure 9. Mean deviation Δ of IGLO/6-31G(d) ^{13}C chemical shifts from experimental values of $C_9H_9^+$ ions located along the C_s search direction. (a) Comparison of average of all nine calculated ^{13}C shift values with experimental value of 118 ppm observed for a completely degenerate rearrangement of **3** at −135 °C. (b) Comparison of 6:3 averages of calculated shift values with experimental values of 101 and 152 ppm measured at −151 °C in the case of a partially degenerate rearrangement of **3**. (c) Comparison of calculated shift values for **3** with those obtained for 9-methyl-**3** and corrected for the effect of a methyl group. (d) The same as curve c but without atoms C2, C8, and C9 (see text). Arrows indicate positions of minimum Δ.

In Figure 9, the mean deviation Δ of IGLO/6-31G(d) ^{13}C chemical shifts from experimental values is plotted as a function of distance $r(4.6)$, i.e. Figure 9 is the chemical shift equivalent of Figure 2, which gives the PES in the C_s search direction. Four different comparisons are made. (a) The time average of all nine

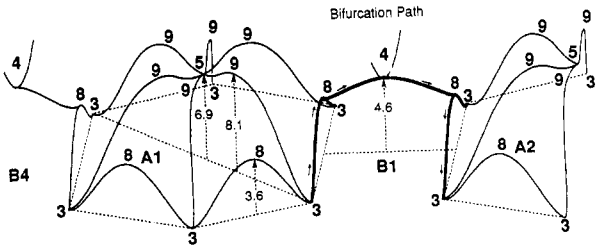

Figure 10. Schematic representation of a section of the MP4(SDQ)/6-31G(d) PES for degenerate rearrangement processes A1, B1, and A2 (compare with Figure 1). For A1, locations of **3**, TSs **8** and **9**, and intermediate form **5** as well as the reaction paths connecting these locations are indicated. The bold lines give the double-bifurcation path of B1 leading from A1 to A2 with **4** as the highest TS. MP4 reaction barriers are given in kcal/mol.

^{13}C shift values is compared with the experimental value of 118 ppm observed for a completely degenerate rearrangement of **3** at −135 °C. (b) A 6:3 time average of calculated shift values is compared with the corresponding experimental values measured at −151 °C (101 and 152 ppm) in the case of a partially degenerate rearrangement. (c) Calculated shift values are compared with those obtained for 9-methyl-**3** and corrected for the effect of a methyl group. (d) A comparison the same as comparison c but without atoms C2, C8, and C9 (see above) is made.

Figure 9 reveals that the best agreement between experimental and calculated ^{13}C chemical shift values (minimum of the mean deviation Δ) is found in comparison a for a distance $r(4,6) = 2.34$ Å, which is close to the MP4 distance of 2.40 Å calculated for **3**. Also in comparisons b, c, and d the minimum of $\Delta = f(r(4,6))$ is found in the region between 2.15 and 2.25 Å, even though the agreement between calculated shifts and experimental estimates is somewhat poorer in these cases. In summary, the shift calculations suggest **3** to be the intermediate of reaction 1 (Scheme II), in agreement with experimental investigations and our MP4-(SDQ) calculations. They also lead to a reasonably accurate location of **3** along the C_s search direction. This nicely demonstrates the usefulness of IGLO chemical shifts in structure determinations.

6. Conclusions

The results of the MP4 investigation of the $C_9H_9^+$ PES in the vicinity of **3** are summarized in Figure 10. They are the basis for the following conclusions: (1) The barbaralyl cation **3** can undergo 30 240 different degenerate rearrangements A, each of which corresponds to a cycle of six divinylcyclopropylcarbinyl cation rearrangements. Rearrangement cycles A are connected by 90 720 fourfold degenerate rearrangement processes B. The PES hosts 181 440 forms of **3** and a total of 272 160 first-order TSs.[23] (2) The sixfold degenerate rearrangement A is the fastest rearrangement process of **3**. It proceeds via reaction path II and TS **8** with an activation energy of 3.6 kcal/mol (MP4(SDQ)/6-31G(d)), which is in excellent agreement with the experimental estimate of 3.8 kcal/mol.[5-8] (3) The fourfold degenerate rearrangement process B proceeds via a double-bifurcation path that connects three first-order TSs, namely TS **8** in one A cycle, TS **8′** in another A cycle and TS **4** at the center between cycles A and A′. According to MP4(SDQ)/6-31G(d) calculations, the activation energy of process B is determined by TS **4**, which is 4.6 kcal/mol higher in energy than **3**. Other possible reaction paths such as IV, V, VI, and VII either are high-energy paths (IVb), forbidden because of symmetry reasons (IVa),[20,21] or do not lead through a first-order TS (V, VI, VII). (4) Rearrangements via path III can contribute to cycle A, but they require an activation energy of 8 kcal/mol, which means that III cannot compete with II at low temperatures. MP4(SDQ)/6-31G(d) results and symmetry rules for TSs[20,21] exclude path IIIa. The reaction must proceed via path IIIb with **9** as a TS and structure

5 as an intermediate. However a detection of 5 by experimental means will not be possible because 5 is sitting in a shallow hollow surrounded by a small-energy ridge with six columns that are the locations of six type-9 TSs. (5) A totally degenerate rearrangement of 3 leading to the equilibration of all nine C atoms requires that 3 proceeds through at least three different A cycles connected via two B processes. The activation energy of this process is given by the activation energy of the double-bifurcation step (4.6 kcal/mol), which is in reasonable agreement with the experimental value of 5.5 kcal/mol.[5-8] (6) Reaction I does not contribute to rearrangement process A, since a Cope intermediate 6 or a TS 7 does not exist. (7) Since MP4 calculations identify 4 as a first-order TS on the PES of $C_9H_9^+$, an experimental detection of 4 will not be possible. However, this does not exclude that an analogue of 4 with a highly localized positive charge is formed in an ion pair during the solvolysis of bicyclo[3.2.2]nona-3,6,8-trien-2-ol or similar compounds. (8) Identification and location of 3 on the PES have also been possible by IGLO/6-31G(d) calculations. Results are in satisfactory agreement with the available experimental data. (9) Calculated MP2/6-31G(d) bond orders reveal the close relationship between 3, 4, 5, and 8. Ion 3 is characterized by four weak CC single bonds and one strong nonbonded interaction that can easily be opened and closed, respectively. Degenerate rearrangements of 3 lead to a relatively small shift of electron density from bond to nonbonded regions, and accordingly, the accompanying energy changes are also relatively small, thus making 3 a highly floppy molecule.

The MP4 exploration of the PES has led to a detailed description of a double-bifurcation reaction mechanism, which is interesting for the symmetry analysis of TS geometries, mechanistic considerations, and reaction dynamics. In addition, our calculations seem to indicate that the McIver–Stanton symmetry rules for TSs[20,21] may be of larger consequence than has been believed so far. Our calculations suggest that a forbidden TS is not avoided by a small vibrational motion but by a significant distortion leading to a well-separated new TS. It seems that the symmetry rules for TSs cannot be outmaneuvered merely by infinitesimally small perturbations of the forbidden geometry.

Acknowledgment. This work was supported by the Swedish Natural Science Research Council (NFR). All calculations were done on the CRAY XMP/416 of the Nationellt Superdatorcentrum (NSC), Linköping, Sweden. The authors thank the NSC for a generous allotment of computer time.